CHAPTER 6

SHAFTS IN LIQUEFIABLE SOILS

6.1 INTRODUCTION

This chapter presents the procedure developed to assess the response of the partially and completely liquefied granular soil as a post-liquefaction analysis. The SW model, initially developed to assess the relationship between one-dimensional beam on elastic foundation (BEF) or so called "p-y" curve behavior and three dimensional soil pile interaction, has been extended to include laterally loaded piles/shafts in liquefiable soil. Because the SW model relies on the undrained stress-strain characterization of the soil as occurs in the triaxial test, it is capable of treating one or more layers of soils that experience limited or full liquefaction. This chapter provides a methodology to assess the post-liquefaction response of an isolated pile/shaft in sand under an applied pile/shaft head load/moment combination assuming undrained conditions in the sand. The degradation in soil strength due to the free-field excess porewater ($u_{xs,ff}$), generated by the earthquake that results in developing or full liquefaction, is considered along with the near-field excess porewater pressure ($u_{xs,\ nf}$) generated by lateral loading from the superstructure.

Current design procedures assume slight or no resistance for the lateral movement of the pile in the liquefied soil which is a conservative practice. Alternatively, if liquefaction is assessed not to occur, some practitioners take no account of the increased $u_{xs,ff}$, and none consider the additional $u_{xs,\ nf}$ due to inertial interaction loading from the superstructure; a practice that is unsafe in loose sands. The paper characterizes the reduction in pile response and the changes in the associated p-y curves due to a drop in sand strength and Young's modulus as a result of developing liquefaction in the sand followed by inertial interaction loading from the superstructure.

The potential of soil to liquefy is one of the critical research topics of the last few decades. Several studies and experimental tests have been conducted for better understanding on the potential of soil to liquefy in both the free- and/or near-field soil regions. However, predicting the response of pile foundations in

liquefied soil or soil approaching liquefaction is very complex.

The procedure presented predicts the post-liquefaction behavior of laterally loaded piles in sand under developing or fully liquefied conditions. Due to the shaking from the earthquake and the associated lateral load from the superstructure, the free field $u_{xs,ff}$ and near-field $u_{xs,nf}$ develop and reduce the strength of loose to medium dense sand around a pile. The soil is considered partially liquefied or experiencing developing liquefaction if the excess porewater pressure ratio (r_u) induced by the earthquake shaking (i.e. $u_{xs,ff}$) is less than 1, and fully liquefied if $r_u = 1$. Therefore, the stress-strain response of the soil due to the lateral push from the pile as the result of superstructure load (and $u_{xs,nf}$) can be as shown in Fig. 6-1. Full-scale load tests on the post-liquefaction response of isolated piles and a pile group, performed at the Treasure Island and Cooper River Bridge (Ashford and Rollins 1999; and S&ME Inc. 2000) presented in Chapter 8, are the most significant related tests. However, the profession still lacks a realistic procedure for the design of pile foundations in liquefying or liquefied soil.

The most common practice employed is that presented by (Wang and Reese 1998) in which The traditional p-y curve for clay is used but based on the undrained residual strength (S_r) of the sand. As seen in Fig. 6-2 (Seed and Harder, 1990), S_r can be related to the standard penetration test (SPT) corrected blowcount, $(N_1)_{60}$. However, a very large difference between values at the upper and lower limits at a particular $(N_1)_{60}$ value affects the assessment of S_r tremendously. Even if an accurate value of S_r is available, S_r occurs at a large value of soil strain. In addition, a higher peak of undrained resistance is ignored in the case of the partially liquefied sand, while greater resistance at lower strain is attributed to the sand in the case of complete liquefaction. Such clay-type modeling can, therefore, be either too conservative (if $r_u < 1$) or unsafe (if $r_u = 1$). Furthermore, the p-y curve reflects soil-pile-interaction, not just soil behavior. Therefore, the effect of soil liquefaction (i.e. degradation in soil resistance) does not reflect a one-to-one change in soil-pile or p-y curve response.

The post-liquefaction stress-strain characterization of a fully or partially liquefied soil is still under investigation by several researchers. The current assessment of the resistance of a liquefied soil carries a

lot of uncertainty. This issue is addressed experimentally (Seed 1979; and Vaid and Thomas 1995) showing the varying resistance of saturated sands under undrained monotonic loading after being liquefied under cyclic loading corresponding to the free-field shaking of the earthquake (Fig. 6-3).

With lateral loading from the superstructure with a significant drop in the confining pressure following full liquefaction or partial liquefaction, the sand responds in a dilative fashion. However, a partially liquefied sand with a small drop in confining pressure may experience contactive behavior followed by dilative behavior under compressive monotonic loading. The post cyclic response of sand, particularly after full liquefaction, reflects a stiffening response, regardless of its initial (static) conditions (density or confining pressure). As seen in Fig. 6-4, there is no particular technique that allows the assessment of the p-y curve and its varying pattern in a partially or fully liquefied sand. Instead, the soil's undrained stress-strain relationship should be used in a true soil-pile interaction model to assess the corresponding p-y curve behavior. Because the traditional p-y curve is based on field data, a very large number of field tests for different pile types in liquefying sand would be required to develop a realistic, empirically based, p-y characterization.

6.2 METHOD OF ANALYSIS

Due to cyclic loading, excess porewater pressure ($\Delta u_c = u_{xs,ff}$) develops and reduces the effective consolidation confining pressure from $\bar{\sigma}_{3c}$ (= $\bar{\sigma}_{vo}$) to $\bar{\sigma}_{3cc}$. As given in Eqn. 6-1, if Δu_c is less than $\bar{\sigma}_{3c}$, sand will be "partially" liquefied and $\bar{\sigma}_{3cc} > 0$. Once Δu_c is equal to $\bar{\sigma}_{3c}$, the sand is completely liquefied (r_u =1) and $\bar{\sigma}_{3cc} = 0$. $\bar{\sigma}_{3cc}$ is the post-cyclic effective confining stress.

$$\bar{s}_{3cc} = \bar{s}_{3c} - \Delta u_c \qquad (6\text{-}1)$$

The degradation in soil resistance due to earthquake shaking and the induced $u_{xs,ff}$ is based on the procedures proposed in (Seed et al. 1983). This $u_{xs,\ ff}$ reduces the effective stress and, therefore, the corresponding soil resistance for subsequent (post cyclic) undrained load application. This is followed by

the assessment of the $u_{xs,\ nf}$ in the near-field soil region induced by the lateral load from the superstructure. The variation in soil resistance (undrained stress-strain relationship) around the pile (near-field zone) is evaluated based on the undrained formulation for saturated sand presented in Ashour and Norris (2000).

The assessed value of the free-field excess porewater pressure ratio, r_u, induced by the earthquake is obtained using Seed's method (Seed et al. 1983). $u_{xs,\ ff}$ is calculated conservatively at the end of earthquake shaking corresponding to the number of equivalent uniform cycles produced over the full duration of the earthquake. Thereafter, the lateral load (from the superstructure) is applied at the pile head that generates additional porewater pressure ($u_{xs,\ nf}$) in the soil immediately around the pile, given the degradation in soil strength already caused by $u_{xs,\ ff}$. Note that $u_{xs,\ ff}$ is taken to reduce the vertical effective stress from its pre-earthquake state ($\bar{\sigma}_{vo}$), to $\bar{\sigma}_v = (1 - r_u)\ \bar{\sigma}_{vo}$. Thereafter, the behavior due to an inertial induced lateral load is assessed using the undrained stress-strain formulation presented in this chapter with the SW model (Ashour and Norris 1999 and 2001; and Ashour et al. 1998).

6.2.1 Free-Field Excess Pore Water Pressure, $u_{xs,\ ff}$

A simplified procedure for evaluating the liquefaction potential of sand for level ground conditions (Seed et al. 1998) is developed based on the sand's corrected SPT blow count, $(N_1)_{60}$. The $u_{xs,\ ff}$ in sand or silty sand soils due to the equivalent history of earthquake shaking can likewise be assessed. The procedure requires knowledge of the total and effective overburden pressure (σ_{vo} and $\bar{\sigma}_{vo}$ respectively) in the sand layer under consideration, the magnitude of the earthquake (M), the associated maximum ground surface acceleration (a_{max}) at the site, and the percentage of fines in the sand. The cyclic stress ratio, CSR [$(\tau_h)_{ave}$ / $\bar{\sigma}_{vo}$], induced by the earthquake at any depth is computed. If N cycles of CSR are induced, but N_L cycles are required to liquefy the sand at this same stress ratio, then the excess porewater pressure ratio (r_u) generated is given as a function of N/N_L. Given r_u, the $u_{xs,\ ff}$ generated and the resulting reduced vertical effective stress are expressed as

$$u_{xs,ff} = r_u\, \bar{s}_{vo} \quad and \quad \bar{s}_v = (1 - r_u)\, \bar{s}_{vo} \tag{6-2}$$

It should be noted that the effect of the pore water pressure in the free field will be considered in the assessment of the t-z curve. As a result, the axial and lateral resistance of the shaft will be affected.

6.2.2 Near-Field Excess Pore Water Pressure, $u_{xs,\ nf}$

The technique developed by Norris et al. (1997) and formulated by Ashour and Norris (1999) employs a series of drained tests, with volume change measurements, on samples isotropically consolidated to the same confining pressure, $\bar{s}_{3c}$, and void ratio, e_c, to which the undrained test is to be subjected. However, the drained tests are rebounded to different lower values of effective confining pressure, $\bar{\sigma}_3$, before being sheared. Such a technique allows the assessment of undrained behavior of isotropically consolidated sand at $\bar{\sigma}_{3c}$ and subjected to compressive monotonic loading (Fig. 6-5, no cyclic loading). During an isotopically consolidated undrained (ICU) test, the application of a deviatoric stress, σ_d, in compressive monotonic loading causes an additional porewater pressure, $\Delta u_d = u_{xs,\ nf}$, that results in a lower effective confining pressure (Fig. 6-5c), $\bar{\sigma}_{3,}$ i.e.

$$\bar{s}_3 = \bar{s}_{3c} - \Delta u_d \qquad \text{(No cyclic loading, near-field pore water pressure only)} \qquad (6\text{-}3)$$

and an associated isotropic expansive volumetric strain, $\varepsilon_{v,iso}$, the same as recorded in an isotropically rebounded drained triaxial test. However, in the undrained test, the volumetric change or volumetric strain must be zero. Therefore, there must be a compressive volumetric strain component, $\varepsilon_{v,\ shear}$, due to the deviatoric stress, σ_d. This shear induced volumetric strain, $\varepsilon_{v,\ shear}$, must be equal and opposite to $\varepsilon_{v,\ iso}$, so that the total volumetric strain, $\varepsilon_v = \varepsilon_{v,\ iso} + \varepsilon_{v,\ shear}$, in undrained response is zero. In the isotropically rebounded drained shear test, $\varepsilon_{v,\ iso}$ and then $\varepsilon_{v,shear}$ (to match $\varepsilon_{v,\ iso}$) are obtained separately and sequentially; in the undrained test, they occur simultaneously (Figs. 6-5a and 6-5b).

$$e_{v,shear} = -e_{v,iso} \qquad (6\text{-}4)$$

During drained isotropic expansion, the resulting axial strain, ε_1, is

$$e_{1,iso} = e_{2,iso} = e_{3,iso} = \frac{1}{3} e_{v,iso} \tag{6-5}$$

Based on Hooke's Law and effective stress concepts (Norris et al. 1998), the undrained axial strain due to shear (σ_d) and effective stress ($\bar{\sigma}_3$) changes can be related to the drained or effective stress strains as

$$(e_1)_{undrained} = (e_1)_{s_d} + (e_1)_{\Delta \bar{s}_3} = (e_1)_{drained} + e_{1,iso} = (e_1)_{drained} + \frac{1}{3} e_{v,iso} \tag{6-6}$$

Therefore, with isotropically consolidated-rebounded drained triaxial tests available for different $\bar{\sigma}_3$, one can assume a value of $\bar{\sigma}_3$, find $\varepsilon_{v,\,iso}$ (Fig. 6-5b), enter the ε_v-ε_1 drained shear curves (Fig. 6-5a) at $\varepsilon_{v,shear}$ equal to $\varepsilon_{v,\,iso}$, and find the drained ε_1 and σ_d on the same confining pressure ($\bar{\sigma}_3$) ε_v-ε_1 and ε_1-σ_d curves. Then $(\varepsilon_1)_{undrained}$ is established according to Eqn. 6-6, and one point on the undrained σ_d-ε_1 curve can be plotted. The corresponding effective stress path ($\bar{p} = \bar{\sigma}_3 + \sigma_d/2$ versus $q = \sigma_d/2$) can also plotted as shown in Fig. 6-5c.

This technique is extended in this paper to incorporate the free-field excess porewater pressure induced by cyclic loading (Δu_c) and its influence on the undrained behavior of sands under the compressive monotonic loading whether the sand is partially or completely liquefied (Fig. 6-1). The following equations account for the pore water pressure in the free- and near-field ($u_{xs,\,ff}$ and $u_{xs,nf}$)

$$\bar{s}_3 = (\bar{s}_{3c} - \Delta u_c) - \Delta u_d = \bar{s}_{3cc} - \Delta u_d$$

($\bar{\sigma}_{3cc} > 0$ and $r_u < 1$ partial liquefaction) (6-7)

$$\bar{s}_3 = \bar{s}_{3c} - \Delta u_c - \Delta u_d = -\Delta u_d$$

($\bar{\sigma}_{3c} = \Delta u_c$, i.e. $\bar{\sigma}_{3cc} = 0$ and $r_u = 1$ complete liquefaction) (6-8)

If $u_{xs,\,ff}$ is equal to $\bar{s}_{3c}$ (i.e. $r_u = 1$), the sand will experience a fully liquefied state ($\bar{s}_{3cc} = 0$) due to the

earthquake shaking . However, the sand is subjected to limited liquefaction when $r_u < 1$.

Based on experimental data obtained by several researchers for different sands, Ashour and Norris (1999) established a set of formulations that allows the assessment of the relationships seen in Figs. 6-5a and 6-5b. These formulations depend on the basic properties of sand and have been modified in this chapter to incorporate the initial effect of cyclic loading and the induced Δu_c on the post-liquefaction behavior of partially or completely liquefied sands.

A. Post-liquefaction Behavior of Partially Liquefied Sands

(` s $_{3cc}$ > 0 or Du$_c$ < ` s $_{3c}$ because r_u <1)

From ABC on the $\varepsilon_{v,\,shear}$-ε_1 curve (Fig. 6-8) and for $\bar{\sigma}_3 < \bar{\sigma}_{3cc}$ (associated with point r and the path r-s - $\bar{r}$ in Figs. 6-6a and 6-6b), the initial slope (S_A), $(\varepsilon_1)_B$ and $(\varepsilon_{v,shear})_{max}$ at point B, and $(\varepsilon_1)_C$ and $(\varepsilon_v)_C$ at point C are assessed based on Eqns. 6-9 through 6-14 (Ashour and Norris 1999).

$$(S_A)_{\bar{s}_{3cc}} = \frac{1}{\exp(r^2 + Dr_c)} \tag{6-9}$$

$$(e_{v,shear})_{B,\bar{s}_{3cc}} = (e_{v,shear})_{\max,\bar{s}_{3cc}} = 2\left[\frac{e^2_{50}}{\exp(Dr_c)}\right]_{\bar{s}_{3cc}} \tag{6-10}$$

$$(e_1)_{B,\bar{s}_{3cc}} = \frac{6\,(e_{v,shear})_{\max,\bar{s}_{3cc}}}{\exp(r\,Dr_c)} \tag{6-11}$$

$$(e_{v,shear})_{C,\bar{s}_{3cc}} = (e_{v,shear})_{\max,\bar{s}_{3cc}}\left[\frac{(e_1)_{B,\bar{s}_{3cc}}}{(e_1)_{C,\bar{s}_{3cc}}}\right]^{0.2}\left[1 + (S_f)_{\bar{s}_{3cc}}\right] \tag{6-12}$$

$$(e_1)_{C,\bar{s}_{3cc}} = 6\,(e_{v,shear})_{\max,\bar{s}_{3cc}} \exp(\tan^2 j) \tag{6-13}$$

$$(S_f)_{\bar{\sigma}_{3cc}} = -\,r^{0.5}\,Dr_c \tan^2 j \tag{6-14}$$

Note that Dr_c (the relative density of consolidation in these equations) is a decimal value.

The empirically calculated slopes and coordinates at points A, B, and C on the ε_1-$\varepsilon_{v,\,shear}$ curve (Fig. 6-8) at $\bar{\sigma}_3 < \bar{\sigma}_{3cc}$ (OCR = $\bar{\sigma}_{3cc} / \bar{\sigma}_3$) are used in the determination of the constants (Eqns. 6-15 through 20 by Ashour and Norris 1999) of the binomial equation that describes the isotropically consolidated rebounded ε_1-$\varepsilon_{v,\,shear}$ curve. The following equations are associated with the path r-s-$\bar{r}$ as seen in Fig. 6-6a.

$$(S_A)_{\bar{\sigma}_3} = \frac{(S_A)_{\bar{\sigma}_{3cc}}}{OCR^{0.5}} \left[\frac{(e_{v,shear})_{\max,\bar{\sigma}_3}}{(e_{v,shear})_{\max,\bar{\sigma}_{3cc}}} \right]^{0.25} \tag{6-15}$$

$$(e_{v,\,shear})_{\max,\bar{\sigma}_3} = \frac{(e_{v,shear})_{\max,\bar{\sigma}_{3cc}}}{OCR^m} \tag{6-16}$$

$$m = r^{0.8} \exp\left[\frac{Dr\ r}{OCR} \right] \tag{6-17}$$

where $OCR = \dfrac{\bar{\sigma}_{3cc}}{\bar{\sigma}_3}$ *for* $\bar{\sigma}_3 \le \bar{\sigma}_{3cc}$; $OCR = \dfrac{\bar{\sigma}_3}{\bar{\sigma}_{3cc}}$ *for* $\bar{\sigma}_3 \ge \bar{\sigma}_{3cc}$

$$(e_1)_{B,\bar{\sigma}_3} = (e_1)_{B,\bar{\sigma}_{3c}} \left[\frac{(e_{v,\,shear})_{\max,\bar{\sigma}_3}}{(e_{v,shear})_{\max,\bar{\sigma}_{3cc}}} \right]^{0.5} \tag{6-18}$$

$$\left(e_{v,shear}\right)_{C,\bar{s}_3} = \left(e_{v,shear}\right)_{\max,\bar{s}_3} \frac{\left(e_{v,shear}\right)_{C,s_{3c}}}{\left(e_{v,shear}\right)_{\max,s_{3c}}} \tag{6-19}$$

$$\left(e_1\right)_{C,\bar{s}_3} = \left(e_1\right)_{C,\bar{s}_{3cc}} \left[\frac{\left(e_1\right)_{B,\bar{s}_3}}{\left(e_1\right)_{B,\bar{s}_{3cc}}}\right]^{0.25} \tag{6-20}$$

$$\left(S_f\right)_{\bar{s}_3} = \left(S_f\right)_{\bar{s}_{3cc}} \tag{6-21}$$

As seen in the above equations, $\bar{\sigma}_{3cc}$ is undertaken as a reference value for OCR. ρ is the sand grain roundness parameter.

- **Isotropically Rebounded and Consolidated Volume Change of Partially Liquefied Sand ($\bar{s}_3$ - $e_{v,iso}$)**

The ($\bar{\sigma}_3$ - $\varepsilon_{v,\,iso}$) relationship seen in Fig. 6-5b is modified to assess the ($\bar{\sigma}_3$ - $\varepsilon_{v,\,iso}$) relationship for sand that has developed partial (limited) liquefaction as the result of cyclic loading (at point r) and been rebounded to point s in Figs. 6-6a and 6-6b. The value of $(\varepsilon_v)_c$ located on the backbone isotropic curve is calculated by Eqn. 6-22.

$$\left(e_v\right)_c = l_7 = e_{50} \exp\left[Dr_c\left(1 + r\right)\right] \tag{6-22}$$

$$e_{v,\,iso} = \left(e_v\right)_c - \frac{\left(e_v\right)_c}{OCR^h} \tag{6-23}$$

$$where \quad h = \frac{r^{0.1}}{4} \exp\left(0.5\, r\, Dr_c\right) \text{ ,and}$$

$$OCR = \frac{\bar{s}_{3cc}}{\bar{s}_3} \quad for \quad \bar{s}_3 \le \bar{s}_{3cc}; \qquad OCR = \frac{\bar{s}_3}{\bar{s}_{3cc}} \quad for \quad \bar{s}_3 \ge s_{3cc}$$

The above procedure can be applied as long the excess porewater pressure ratio (r_u) induced by cyclic loading is less than 1 and the residual confining pressure ($\bar{\sigma}_3$) is greater than zero at point r (partially liquefied soil). Under monotonic loading, the partially liquefied sand may then experience a contractive response associated with a reduction in $\bar{\sigma}_3$ (from point r to point s in Figs. 6-6a and 6-6b) to reach the lowest value of $\bar{\sigma}_3$, and then rebound (dilate) with increasing $\bar{\sigma}_3$ until $\bar{\sigma}_3 = \bar{\sigma}_{3cc}$ again (point $\bar{r}$ in Figs. 6-6a and 6-6b). Sand continues to dilate beyond $\bar{\sigma}_{3cc}$ (Figs. 6-6a and 6-6b) with increasing $\bar{\sigma}_3$ and net negative porewater pressure. It should be noted that when $\bar{\sigma}_3 < \bar{\sigma}_{3cc}$, $\varepsilon_{v,iso}$ rebounds to point s and then recompresses. This is associated with an equal net compressive $\varepsilon_{v,shear}$. However, when $\bar{\sigma}_3 > \bar{\sigma}_{3cc}$, $\varepsilon_{v,iso}$ moves from $\bar{r}$ to $\bar{s}$ and an equal dilative $\varepsilon_{v,shear}$ develops simatanuously. In the undrained test, the volume change or volumetric strain must be zero such that at all times $\varepsilon_{v,iso} = -\varepsilon_{v,shear}$.

As applied in Fig. 6-5a, ε_1 associated with $\Delta\bar{s}_3$ and $\varepsilon_{v,shear}$ represents the current drained axial strain. Based on Eqns. 6-5 and 6-6, the drained ε_1 is converted to the undrained ε_1. The associated deviator stress (σ_d) is determined as follows,

$$s_d = SL\left(s_d\right)_f = \bar{s}_3\left[\tan^2\left(45 + \frac{j}{2}\right) - 1\right] \tag{6-24}$$

The varying stress level (SL) is a function of ε_1, ε_{50}, and $\bar{\sigma}_3$ as presented by Ashour and Norris (1999).

B. Post-liquefaction Behavior of Completely (Fully) Liquefied Sands

(` $s_{3cc}$ = 0 or $u_c$ = ` s_{3c} and r_u = 1)

Once the soil is completely liquefied (i.e. r_u =1, $\bar{\sigma}_3$ and σ_d are equal to zero) due to cyclic loading, the above procedure must be modified in order to handle a different type of behavior. As seen in Fig. 6-3, the completely liquefied soil loses its strength when the excess porewater pressure due to cyclic loading is equal

to the effective confining pressure ($u_{xs} = \Delta u_c = \bar{\sigma}_{3c}$) and the porewater pressure ratio (r_u) = 1. By applying monotonic loading thereafter, u_{xs} decreases and causes a growth in confining pressure (effective stress). This will be accompanied by a growth in sand resistance (σ_d).

As seen in Fig. 6-3 beyond a certain value of strain ($\varepsilon_1 = x_o$; $x_o \cong 20\%$ in the figure), u_{xs} decreases to zero and then to negative values. At $u_{xs} = 0$, sand exhibits resistance that is equal to that of initial loading at the same zero porewater pressure. Once u_{xs} becomes negative, $\bar{\sigma}_3$ will be larger than $\bar{\sigma}_{3c}$ and the undrained resistance will be greater than the drained strength.

Based on its Dr_c, the completely liquefied sand may experience a zero-strength transition zone with soil strain ($\varepsilon_1 \leq x_0$) and $r_u = 1$ before it starts to show some resistance, confining pressure ($\bar{\sigma}_3$) and dilative response (Fig. 6-3). This value of x_0 decreases with the increase of the sand relative density (D_r) and becomes approximately zero for dense sand.

As a result of the development of complete liquefaction by cyclic loading and the subsequent dilative response under an isotopically consolidated undrained (ICU) loading, two equal and opposite components of volume change (strain) develop in sand. In the undrained test, the total volumetric change or volumetric strain must be zero. Therefore, the shear induced volumetric strain, $\varepsilon_{v,\ shear}$, must be equal and opposite to $\varepsilon_{v,\ iso}$ (Eqn. 6-4). In the isotropically rebounded drained shear test, $\varepsilon_{v,\ iso}$ and then $\varepsilon_{v,\ shear}$ (to match $\varepsilon_{v,\ iso}$) are obtained separately and sequentially; in the undrained test, they occur simultaneously.

Figure 6-7 shows the drained dilative response of sand when $\varepsilon_{v,shear}$ is expansive and $\varepsilon_{v,\ iso}$ is compressive starting with $\bar{\sigma}_3 = 0$. As a result of the complete liquefaction under cyclic loading, $\bar{\sigma}_3 = \bar{\sigma}_{3cc} \cong 0$ (point r in Figs. 6-7a and 6-7b) and the associated $\varepsilon_{v,iso}$ at the start of undrained monotonic loading (point $\bar{r}$ in Figs. 6-7a and 6-7b). The change in the volumetric strain $\varepsilon_{v,\ iso}$ due the increase in $\bar{\sigma}_3$ is represented by the variation in $\varepsilon_{v,\ iso}$ (Fig. 6-7a) associated with $(\varepsilon_{v,shear})_{net\ dilative}$ in Fig. 6-7c. Equation 6-23 for $\varepsilon_{v,iso}$ is modified as follows:

$$e_{v,iso} = \frac{(e_v)_c}{OCR^h} - (e_{v,iso})_a \tag{6-25}$$

and

$$(e_{v,iso})_a = \frac{(e_v)_c}{(OCR^h)_{at\ Point\ \bar{r}}} \qquad where \quad OCR = \frac{\bar{s}_{3c}}{\bar{s}_3}$$

It should be noted that $\bar{\sigma}_3$ at point ($\bar{r}$) is approximately equal to zero. As observed experimentally and based on its relative density, the liquefied sand may experience a zero-resistance zone ($\bar{\sigma}_3 = 0$ and $\sigma_d = 0$) with a progressive axial strain (up to $\varepsilon_1 = x_0$) under the compressive monotonic loading. x_0 is determined from the drained rebounded ε_1-$\varepsilon_{v,shear}$ relationship at very small values of $\bar{\sigma}_3 \cong 0$ (Fig. 6-7). x_0 defines the end of complete liquefaction zone ($\Delta u_c = \bar{\sigma}_{3c}$) and indicates the subsequent growth in $\bar{\sigma}_3$ and σ_d, the degradation in the excess porewater pressure (Fig. 6-7a), and the development of dilative response (Fig. 6-7c). It should be noted that $\varepsilon_{v,shear}$ for the dilative sand represents the suppressed volume increase beyond the original volume of sand.

As seen in Fig. 6-7b, the resistance of completely liquefied sand under compressive monotonic loading lies on the failure envelope with stress level (SL) equal to 1. The variation of sand resistance after complete liquefaction due to its dilative response is a function of the varying $\bar{\sigma}_3$ and the full friction angle φ.

$$s_d = SL\,(s_d)_f = \bar{s}_3\left[\tan^2\left(45 + \frac{j}{2}\right) - 1\right] \tag{6-26}$$

It should be noted that the values of the post-liquefaction response of sand depend on the magnitude of $\bar{\sigma}_3$ remaining after cyclic loading (Vaid and Thomas 1995).

6.3 CASE STUDIES

The approach developed here to assess the post-liquefaction behavior of liquefied sands has been verified through various comparisons to experimental results of different types of sands under monotonic loading

after being completely or partially liquefied by cyclic loading. The properties of these sands are presented in Table 6-1.

6.3.1 Post-Liquefaction Response of Completely Liquefied Nevada Sand

Figure 6-9 shows the good agreement between the measured and predicted post liquefaction resistance of Nevada sand under compressive monotonic loading. The sample tested was isotropically consolidated to $\bar{\sigma}_{3c}$ = 400 kPa at Dr_c = 15% and exhibited a drained $\varphi = 32^o$ and ε_{50} = 0.0065. The sample was completely liquefied by cyclic loading and then the undrained response shown in Fig. 6-9 was obtained (Nguyen 2002).

6.3.2 Post-Liquefaction Response of Completely Liquefied Ione Sand

Figure 6-10 shows the observed and predicted post-liquefaction response of Ione sand. Dr_c = 30%, for an isotropic consolidation pressure ($\bar{\sigma}_{3c}$) of 800 kPa and $\varphi = 29^o$ and ε_{50} = 0.008 in drained tests. Similar to Nevada sand, Ione sand was completely liquefied by cyclic loading and then subject to compressive monotonic loading (Nguyen 2002).

6.3.3 Post-liquefaction Response of Partially and Completely Liquefied Fraser River Sand

Vaid and Thomas (1995) performed a set of cyclic and then compressive monotonic loading tests to study the effect of residual confining pressure ($\bar{\sigma}_3$) on the post liquefaction behavior of a completely ($\bar{\sigma}_3 = 0$) and partially liquefied ($\bar{\sigma}_3 > 0$) Fraser sand. There is very good agreement between observed and predicted results in Fig. 6-11. The results shown in Fig. 6-11 for Fraser sand were obtained based on the completely liquefied status ($\bar{\sigma}_3 = 0$) for different Dr_c (Vaid and Thomas 1995).

Figure 6-12 shows the influence of partial or limited liquefaction induced by cyclic loading ($\bar{\sigma}_3 > 0$) on the post liquefaction behavior of 40% relative density samples of Fraser sand. The pre-cyclic consolidation pressure ($\bar{\sigma}_{3c}$) was 400 kPa, and the residual confining pressures induced by cyclic loading were 105 and 45 kPa, respectively.

6.4 UNDRAINED STRAIN WEDGE MODEL FOR LIQUEFIED SAND

The basic purpose of the SW model is to relate stress-strain-strength behavior of the soil in the wedge to one-dimensional Beam on Elastic Foundations (BEF) parameters. The SW model is, therefore, able to provide a theoretical link between the more complex three-dimensional soil-pile interaction and the simpler one-dimensional BEF characterization. As presented in Chapter 5, the SWM is based on the mobilized passive wedge in front of the pile (Fig. 6-13) which is characterized by base angle, β_m, the current passive wedge depth, h, and the spread of the wedge via the fan angle, φ_m (the mobilized effective stress friction angle). The horizontal stress change at the passive wedge face, $\Delta\sigma_h$, and side shear, τ, act as shown in Fig. 6-13.

The varying depth, h, of the deflected portion of the pile is controlled by the stability analysis of the pile under the conditions of soil-pile interaction. The effects of the soil and pile properties are associated with the soil-pile reaction along the pile via the Young's modulus of the soil (E), the stress level in the soil (SL), the pile deflection (y), and the modulus of subgrade reaction (E_s) between the pile segment and each soil sublayer (Chapter 5).

The shape of the wedge in any soil layer depends upon the properties of that layer and, therefore, would seem to satisfy the nature of a set of independent Winkler soil springs in BEF analysis. However, the mobilized depth (h) of the passive wedge at any time is a function of the various soils (and their stress levels) and the bending stiffness (EI) and head fixity condition of the pile. This, in turn, affects the resulting p-y response in a given soil layer; therefore, the p-y response is not a unique function of the soil alone. The governing equations of the mobilized passive wedge shape are applied within each soil sublayer (i) of a given deposit. The configuration of the wedge (Fig. 6-13) at any instant of load is a function of the stress level in the sublayer of sand and, therefore, its mobilized friction angle, φ_m. Note that

$$(\beta_m)_i = 45 + \frac{(\varphi_m)_i}{2}, \qquad \text{and}$$

$$\left(\overline{BC}\right)_i = D + (h - x_i)\,2\left(\tan \beta_m\right)_i \left(\tan \phi_m\right)_i \qquad (6\text{-}27)$$

where $\overline{BC}$ is the width of the wedge face at any depth. h symbolizes the current full depth of the passive wedge in front of the pile; x_i represents the depth from the top of the pile or passive wedge to the middle of the sublayer under consideration; and D indicates the width of the pile cross-section (Fig. 6-13). As presented in Chapter5, the geometry of the passive wedge(s) (short, intermediate or long shafts) is a function of the state of the soil. Consequently, the developing passive wedge in the liquefiable soil will be different from its original (as-is conditions) case under drained conditions.

Under undrained conditions, the major principal stress change ($\Delta\sigma_h$) in the wedge is in the direction of pile movement, and it is equivalent to the deviatoric stress (σ_d) in the isotropically consolidated undrained (ICU) triaxial test. Assuming that the horizontal direction in the field is taken as the axial direction in the triaxial test, the vertical stress change ($\Delta\sigma_v$) is zero and the perpendicular horizontal stress change ($\Delta\sigma_{ph}$) is taken to be the same. Corresponding to the (ICU) triaxial compression test, the deviatoric stress is increased, while the effective confining pressure decreases due to the positive induced excess porewater pressure, Δu_d. Note that Δu_d represents $u_{xs,nf}$ in the near-field region. The cycles of earthquake loading will generate excess porewater pressure in the free-field ($u_{xs,\,ff}$) that will reduce the effective stress in sand (Eqns. 6-1 and 6-2) according to its location below ground surface. Once the excess porewater pressure ($u_{xs,nf}$) increases due to the pile loading, the confining pressure in the sand around the pile reduces to

$$\bar{\sigma}_v = \bar{\sigma}_3 = (\sigma_{3c} - u_{xs,\,ff}) - u_{xs,nf} \quad \textit{where} \quad \bar{\sigma}_h = \bar{\sigma}_v + \Delta\sigma_h \qquad (6\text{-}28)$$

$u_{xs,\,nf}$ (= Δu_d) is a function of stress level. Therefore, the assessment of the mobilized resistance of the sand (σ_d = $\Delta\sigma_h$) as a function of the axial strain (major strain) under undrained conditions allows the determination of the sand resistance and pile deformation at the associated undrained horizontal strain, ε_u. The current value of undrained Young's modulus in sand sublayer (i) which is associated with ε_u is given as

$$(E_u)_i = \left[\frac{\Delta s_h}{e_u}\right]_i = \left[\frac{s_d}{e_u}\right]_i \tag{6-29}$$

$$SL_i = \left[\frac{\Delta s_h}{\left(\Delta s_{hf}\right)_{\bar{s}_3}}\right]_i = \frac{(s_d)_i}{(\bar{s}_3)_i\left[\tan^2\left(45+\frac{j_i}{2}\right)-1\right]}$$

$$= \frac{\tan^2\left(45+\frac{(j_m)_i}{2}\right)-1}{\tan^2\left(45+\frac{j_i}{2}\right)-1} \tag{6-30}$$

The major principal effective stress change, $\Delta\sigma_h$, in the passive wedge is in the direction of pile movement and is equivalent to the deviatoric stress change in the undrained triaxial test, σ_d (assuming that the horizontal direction in the field is taken as the axial direction in the triaxial test). The mobilized effective stress fanning angle, φ_m, of the passive wedge is related to the stress level or the strain in the sand. Knowing the soil strain, ε_u, the deviatoric stress, σ_d, and the associated instant effective confining pressure, $\bar{\sigma}_3$. φ_m can be determined from the associated effective stress-strain curve and effective stress path. Based on the approach presented in (Ashour and Norris 1999 and 2001), both the stress level, SL, and the mobilized angle of internal friction, φ_m, associated with the effective stress, $\bar{\sigma}_3$, and soil strain, ε_u, under undrained conditions can be calculated. Stress level (SL) relates σ_d (= $\Delta\sigma_h$) to σ_{df} (= $\Delta\sigma_{hf}$); where $\Delta\sigma_{hf}$ is the peak of the associated drained (i.e. current $\bar{\sigma}_3$) effective stress-strain curve.

The initial and subsequent values of confining pressure are not equal along the depth of the passive wedge of sand in front of the pile. Therefore, at the same value of horizontal soil strain (ε_u), the undrained resistance of the sand surrounding the pile varies throughout the depth of the passive wedge of sand providing different values of stress level. Such behavior requires the determination of the mobilized undrained resistance of the sand along the depth of the passive wedge. The SW model provides the means to divide the sand layer into equal-thickness sublayers in order to calculate the undrained sand response of each sublayer (i) according to the location and the properties of sand of that sublayer.

6.5 SOIL-PILE INTERACTION IN THE SW MODEL UNDER UNDRAINED CONDITIONS

By applying the drained SW model procedures for granular soil (Chapter 5), the modulus of subgarde reaction of sand under undrained conditions (E_{su}) at any sublayer (i) can be determined based on the associated values of E_u and SL. The SW model relies on calculating E_{su}, which reflects the soil-pile interaction at any level during pile loading or soil strain. By comparison with the drained E_s, in drained sand (Ashour et al. 1998), E_{su} is given in any sublayer (i) as

$$(E_{su})_i = \frac{p_i}{y_i} = \frac{D(A\varepsilon_u E_u)_i}{\delta(h - x_i)} = \frac{(A E_u)_i}{(h - x_i)} D(\Psi_u) \qquad (6\text{-}31)$$

Corresponding to a horizontal slice of (a soil sublayer) at a depth x (Fig. 6-13) under horizontal equilibrium, the soil-pile reaction, the undrained p_i (line load) is expressed as a function of $\Delta\sigma_h$ where $\Delta\sigma_h$ represents the mobilized undrained resistance in sand sublayer (i).

$$p_i = (\Delta\sigma_h)_i \overline{BC}_i S_1 + 2\tau_i D S_2 \qquad (6\text{-}32)$$

Shape factors S_1 and S_2 are equal to 0.75 and 0.5, respectively, for a circular pile cross section, and equal to 1.0 for a square pile; τ is shear stress along the sides of the pile. A is a parameter that governs the growth of the passive soil wedge and based on the concepts presented in Chapter 5. ψ_u is equal to 1.55 where the total stress Poisson's ratio for undrained sand is equal to 0.5. Equation 6-31 is based upon the undrained response of sand using the undrained stress-strain relationship (ε_u, σ_d and E_u). Once the values of E_{su} at any level of loading along the length of the deflected portion of the pile are calculated, the laterally loaded pile and the three-dimensional passive wedge in front of the pile can be transformed into a BEF problem and solved using a numerical technique such as the finite element method. The evaluation of E_{su}

as a function of soil and pile properties is the key point to the SW model analysis.

6.6 SUMMARY

The procedure presented yields the undrained lateral response of a laterally loaded pile/shaft in liquefiable soil incorporating the influence of both the developing excess porewater pressure in the free-field $u_{xs,\ ff}$ (due to ground acceleration) and the additional $u_{xs,\ nf}$ (due to the lateral load from the superstructure). The technique reflects the effect of soil liquefaction on the assessed (soil-pile reaction) p-y curves based on the reduced soil-pile interaction response (modulus of subgrade reaction). The capability of this procedure will (1) reduce the uncertainty of dealing with the behavior of laterally loaded piles in liquefiable soils and (2) allow estimation of realistic responses of laterally loaded piles in liquefiable soils based that properly account for local site conditions and shaft properties as demonstrated by the predictions for the Treasure Island and Cooper River Bridge load tests presented in Chapter 8.

Table 6-1. The properties of sands employed to demonstrate the approach presented

Material	Roundness (ρ)	e_{max}	e_{min}	C_u	Ref.
Nevada Sand (subrounded, clean, fine, white quartz, foundry sand)	0.45	0.856	0.548	1.6	Norris et al. (1995, 1997)
Ione Sand (subangular, clean, minerals, quartz, glass sand)	0.29	1.00	0.717	1.4	Norris et al. (1995, 1997)
Fraser River Sand (subangular to subrounded well graded quartz and feldspar sand)	0.4	1.00	0.68	1.5	Fukushima and Tatsuoka. (1984)

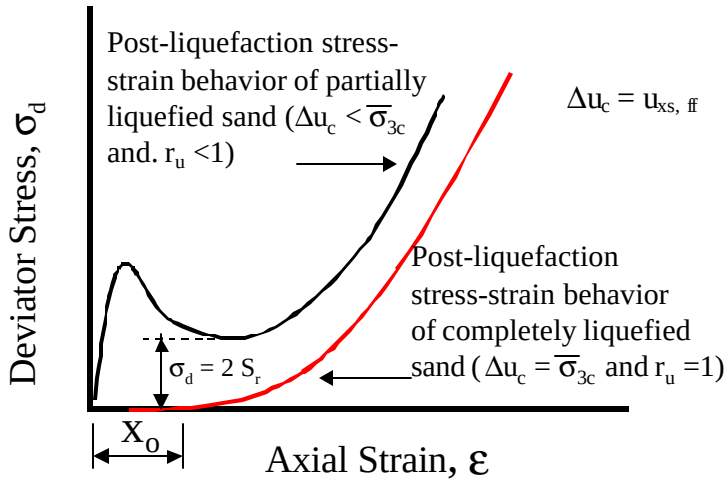

Fig. 6-1 Subsequent Undrained Stress-Strain Behavior of Sand that has Experienced Partial (r_u <1) or Complete (r_u =1) Liquefaction

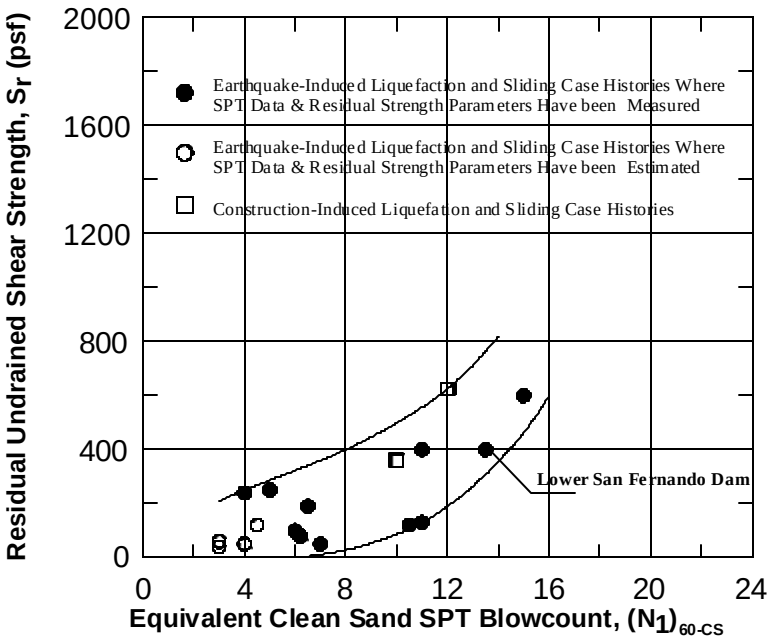

Fig. 6-2 Corrected Blowcount vs. Residual Strength (Seed and Harder, 1990)

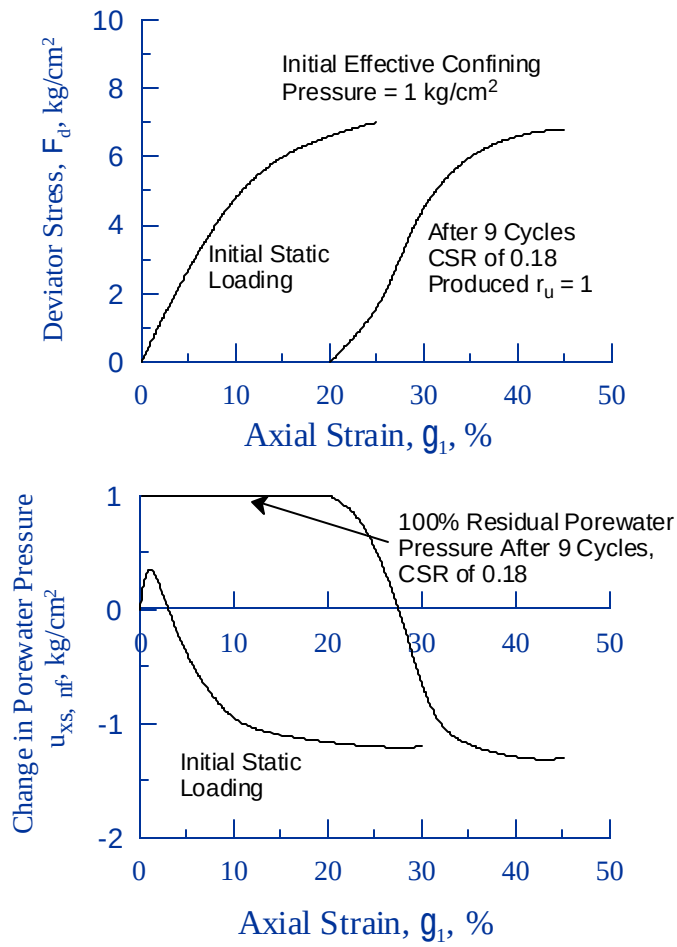

Fig. 6-3 Undrained Behavior of Sacramento Sand under Initial Static and Fully Liquefied Conditions (Seed 1979)

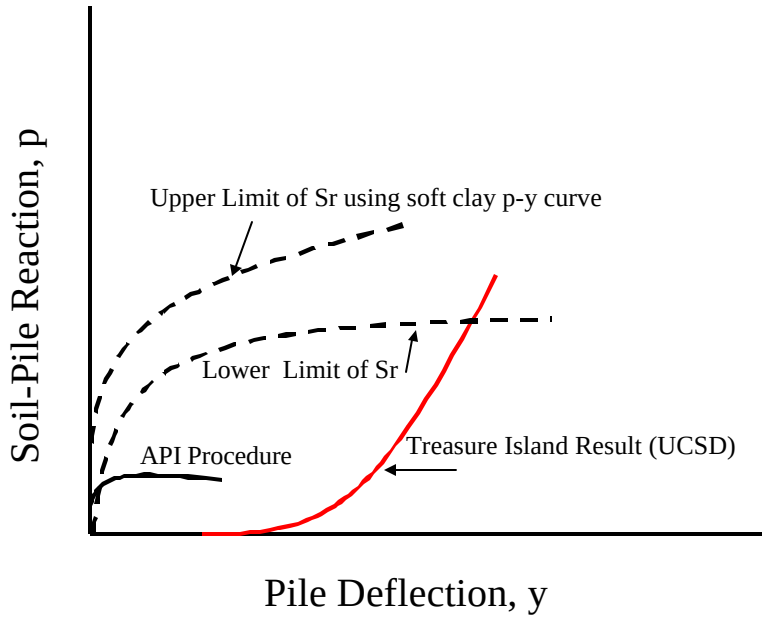

Fig. 6-4 Undrained p-y Curve in Liquefied Soil (Rollins et al. 2001)

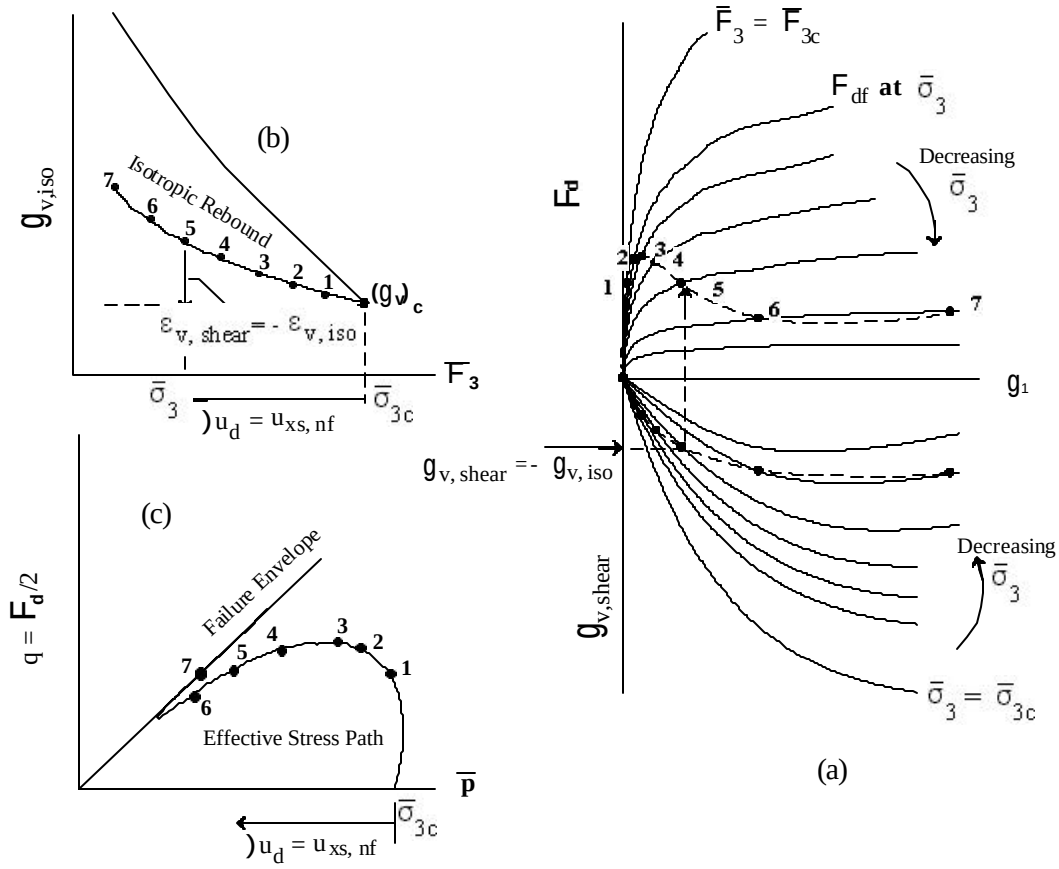

Fig. 6-5 Interrelationships Among
(a) Drained and Undrained Stress-Strain Behavior
(b) Isotropic Consolidation Rebound, and
(c) Undrained Effective Stress Path (Norris et al. 1997)

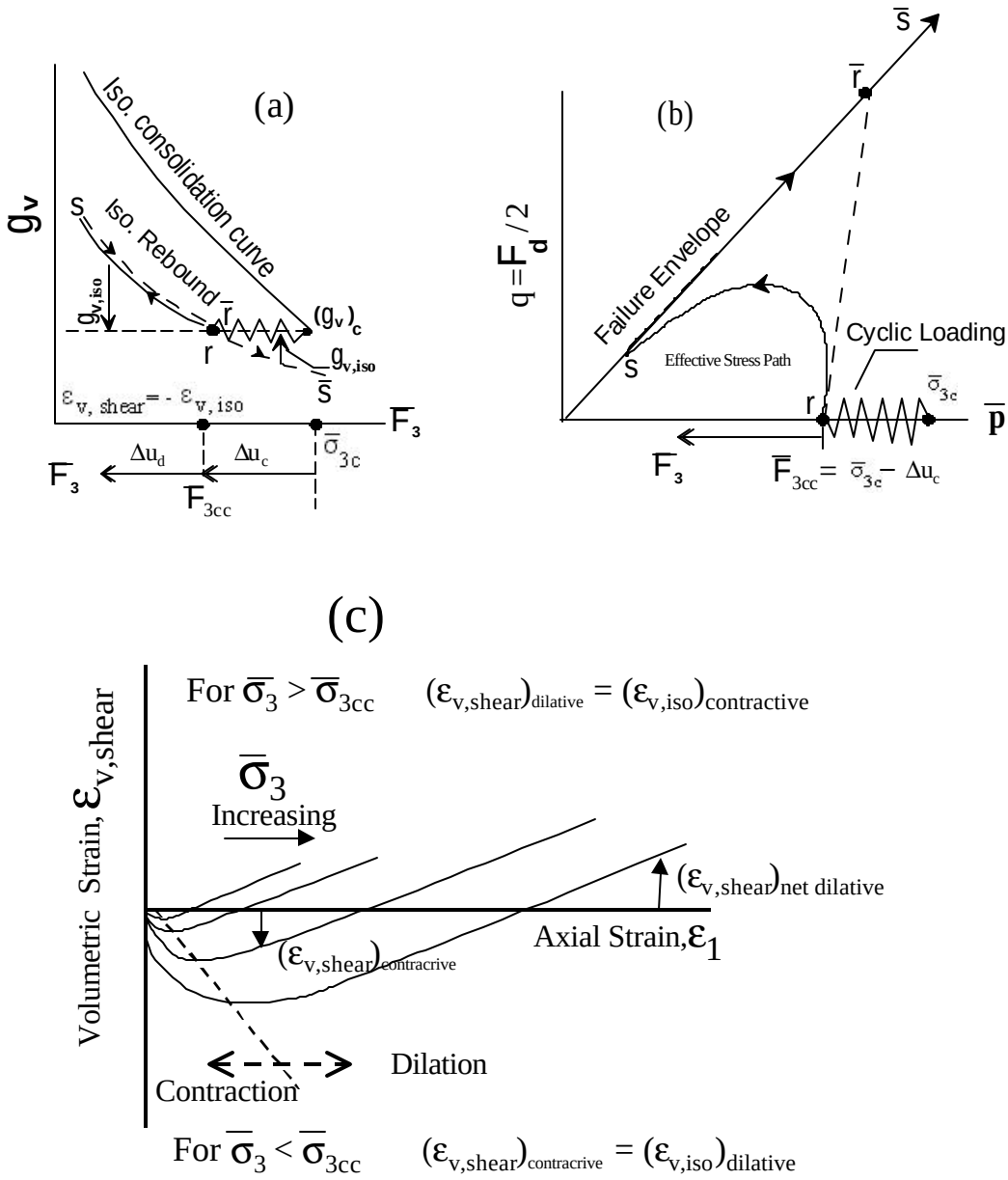

Fig. 6-6 Fully Liquefied Sand Interrelationships Among
(a) Isotropic Consolidation Followed by Cyclic Loading
(b) Undrained Effective Stress Path, and
(c) Drained Volumetric-Axia; Srain Behavior under Different Values of ` s 3

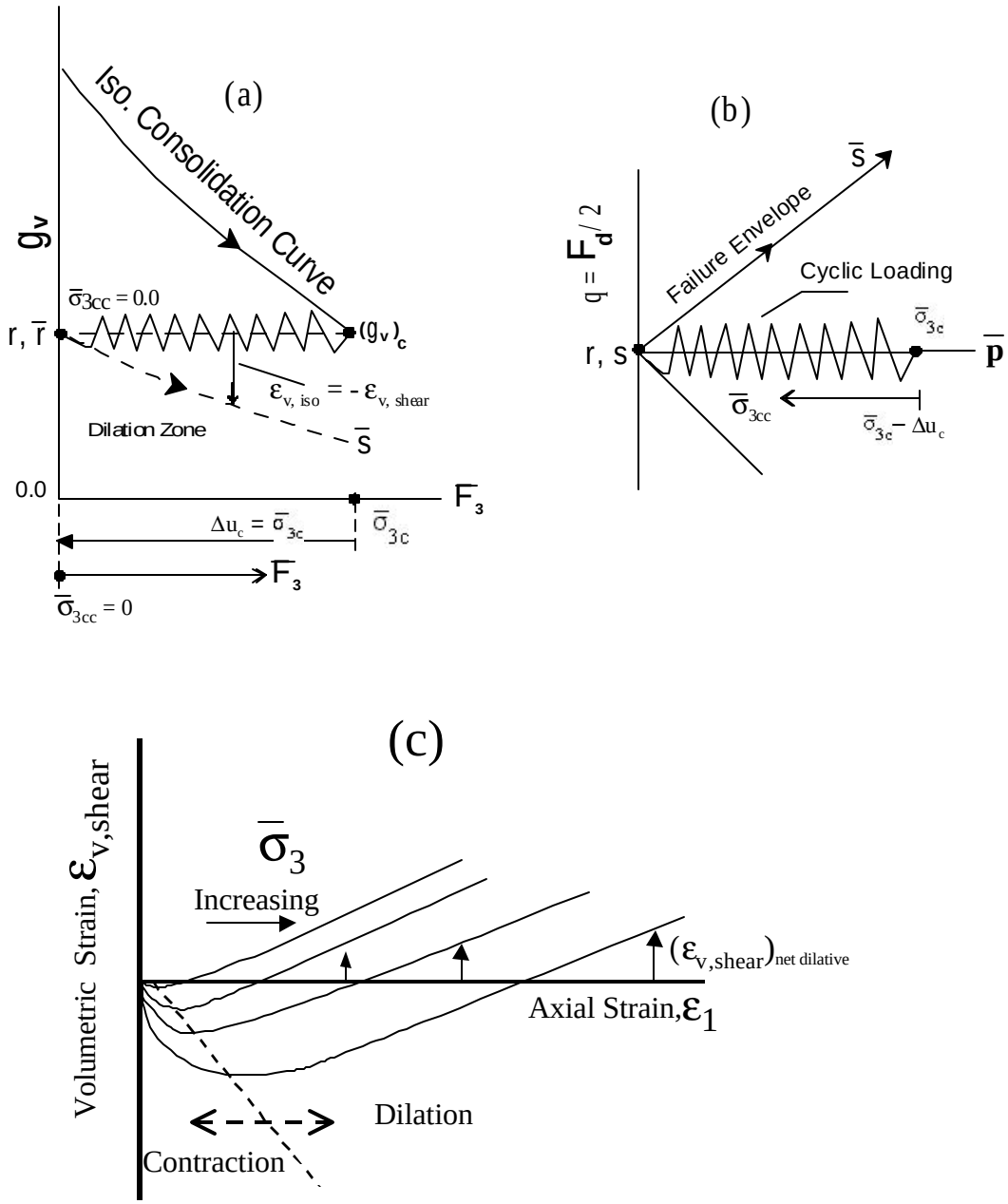

At the same $\bar{\sigma}_3$ $\quad (\varepsilon_{v,shear})_{dilative} = (\varepsilon_{v,iso})_{contractive}$

Fig. 6-7 Limited Liquefied Sand Interrelationships among
(a) Isotropic Consolidation Followed by Cyclic Loading (r_u <1)
(b) Undrained Effective Stress Path, and
(c) Drained Volumetric-Axial Strain Behavior under Different Values of Rebounded $\bar{s}_3$

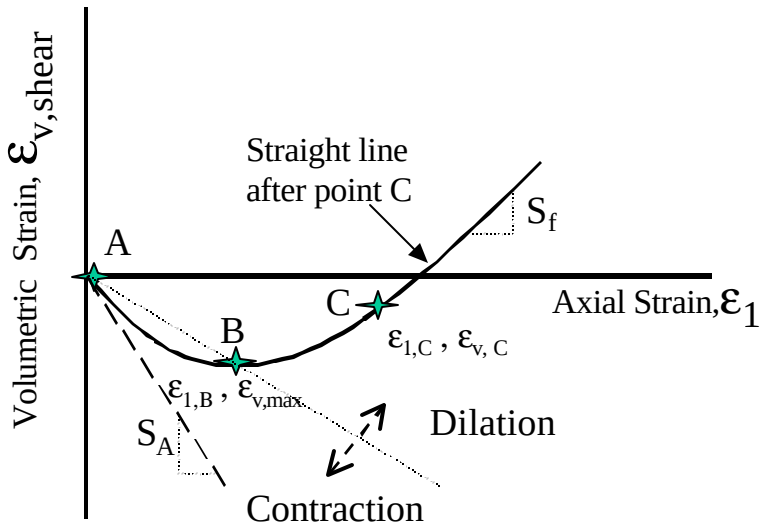

Fig. 6-8 Volumetric strain curve and its major points

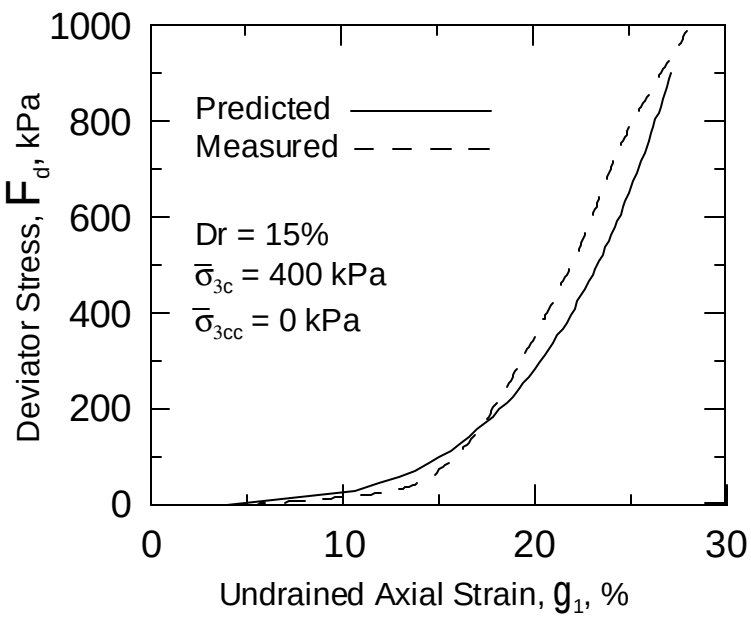

Fig. 6-9 Post-Liquefaction Undrained Stress-Strain Behavior of Completely Liquefied Nevada Sand

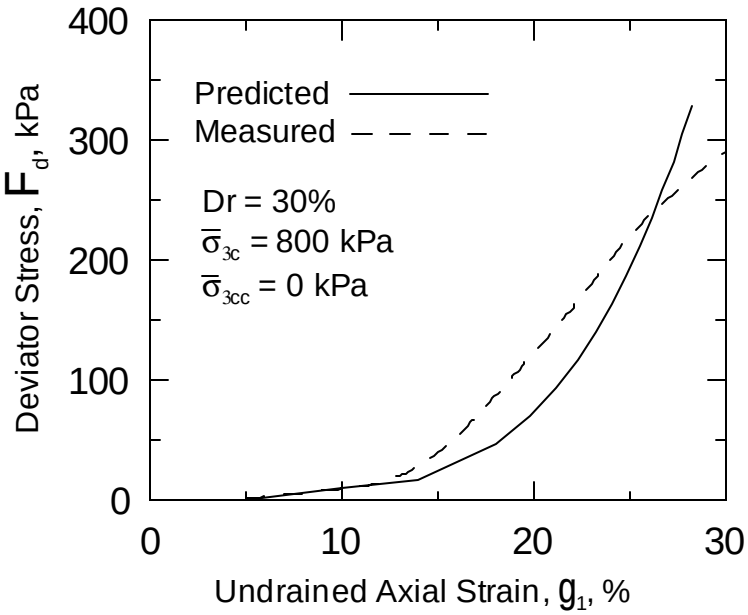

Fig. 6-10. Post-Liquefaction Undrained Stress-Strain Behavior of Completely Liquefied Ione Sand

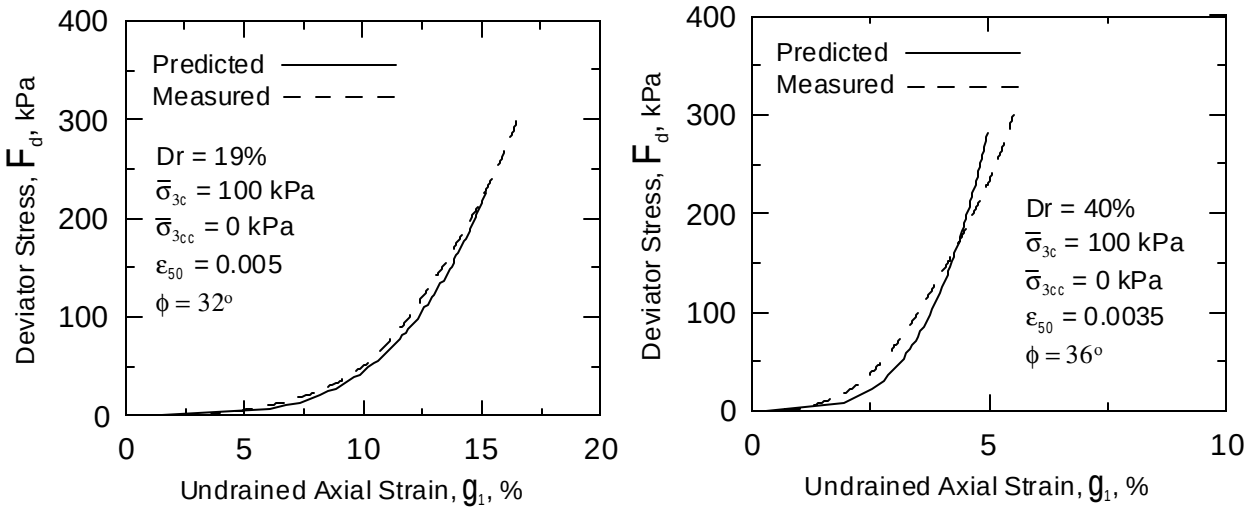

Fig. 6-11 Post-Liquefaction Undrained Stress-Strain Behavior of Completely Liquefied Fraser Sand

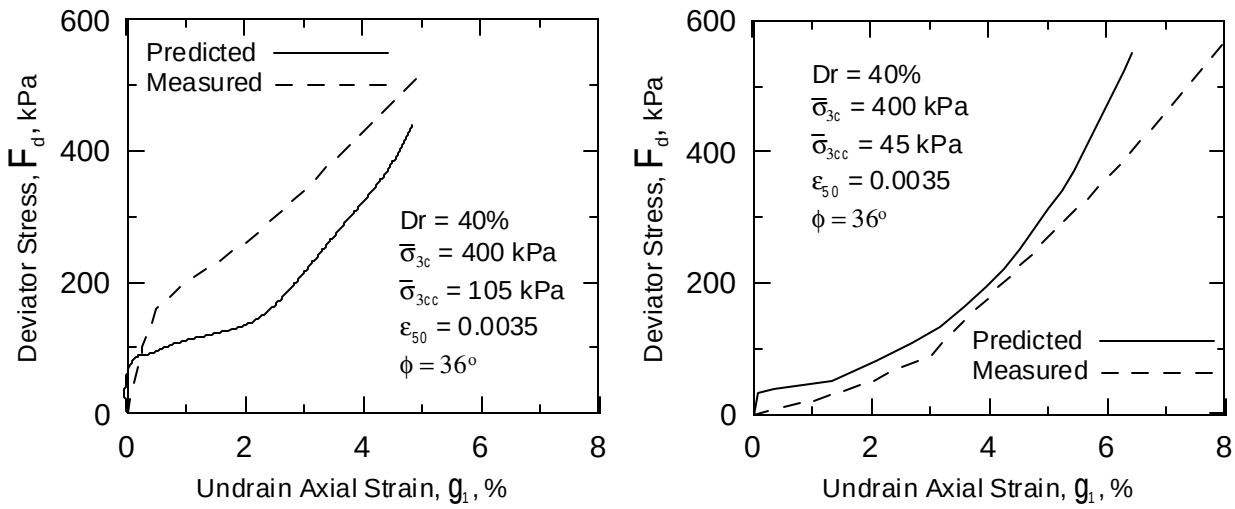

Fig. 6-12 Post-Liquefaction Undrained Stress-Strain Behavior of Partially Liquefied Fraser Sand

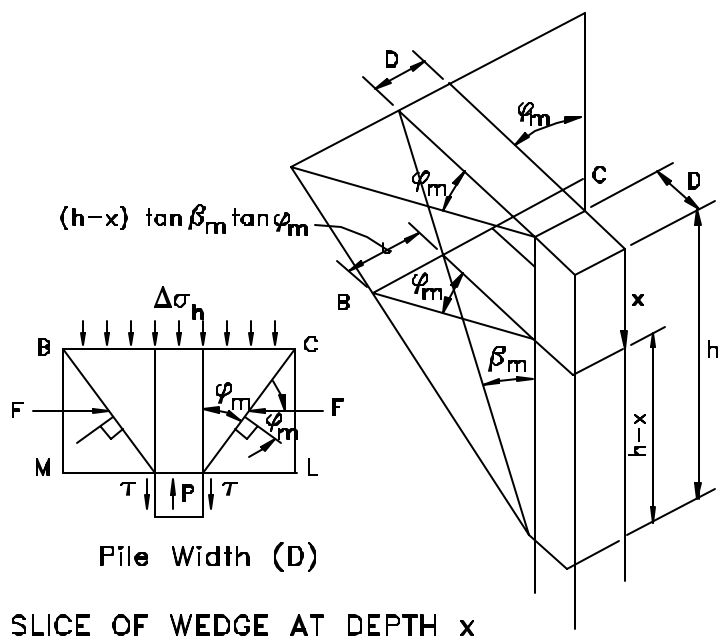

Fig. 6-13 Basic Characterization of the Strain Wedge Model (SW Model)